Analysis of Hydrogen-Induced Degradation Dynamics From Femtoseconds to Gigaseconds in Silicon Heterojunction Solar Cells with Machine Learning Methods

Supplemental Material

Si-H GAP

A full description of the training and validation protocols are available in reference [1].

DFT

The DFT calculations were performed using the Quantum Espresso 6.2.1 software package [2–4], with the key parameters as follows. The Perdew-Burke-Ernzerhof (PBE) exchange-correlation functional was used with periodic boundary conditions [5]. The core and valence electron interactions were described by the Norm-Conserving Pseudopotential function. The calculations were performed with Marzari-Vanderbilt electronic smearing [6]. This smearing method was chosen as it ensures that the DFT energies and forces are consistent, and the electronic free energy was used as the "energy" training target, because its derivatives with respect to the atomic positions are reported as "forces" by the DFT code (according to the Hellman-Feynman theorem). An energy cutoff of 42 Ry was employed for the plane-wave basis set, and a Monkhorst-Pack grid method was used to define the k-point mesh which samples the Brillouin-Zone. The k-point spacing was chosen to be 0.2Å^{-1}.

DFT optimization

We used the Broyden-Fletcher-Goldfarb-Shanno (BFGS) quasi-newton algorithm, based on the trust radius procedure as the optimization algorithm. The Perdew-Burke-Ernzerhof (PBE) exchange-correlation functional [5] was used in both the ionic relaxation and the electronic structure calculations using periodic boundary conditions. The core and valence electron interactions were described by the Norm-Conserving Pseudopotential function. Unless otherwise stated, an energy cutoff of 12 Ry was employed for the plane-wave basis set and a 2×2×2 k-point mesh was used with the Monkhorst-Pack grid method for the Brillouin-zone sampling in all the calculations. Methfessel-Paxton smearing [7] of width 0.05 Ry was applied to determine the band occupations and electronic density of states.

NEB

Parameter Convergence

The nudged elastic band (NEB) method as implemented by LAMMPS provides an extremely efficient and highly versatile platform for computing a wide variety of events; however, the high versatility comes at a cost of a high number of tunable parameters: nine. Before measuring the energy barriers of the four processes described in the main text, we preformed a series of calculations for the migration of a vacancy in c-Si, a process that had been previously simulated using multiple techniques, including using NEB with a Si GAP. Table 1 shows the activation energy for this process as reported by previous studies, as well as our own calculations using some of the standard empirical Si potentials. To perform these simulations we created a 2x2x3 primitive unit cells simulation box containing 56 - 1 Si atoms in a diamond lattice. We created initial and final states by moving the vacancy to an adjacent site. Our

Table 1: **Energy Barrier for Si Vacancy Migration**

Method	E_A
Experiment	$0.45 \pm 0.04eV$[8, 9]
DFT	$0.30eV$[10]
GAP	0.22[10]
SW	0.308
Tersoff	2.113

initial simulation yielded a forward energy barrier ,FE_A(eV), of 0.368 eV and a reverse energy barrier, RE_A(eV), of 0.240 eV.

The inconsistency of the forward and reverse barriers seen in the calculation of vacancy migration by Si GAP appeared to be the result of the specific atoms included in neb calculation. The method we used selected a group of NEB atoms by defining a cubic region around the reaction site and including the atoms within that region, while any others were frozen in place. To investigate the issue considering the uneven barriers we preformed simulations using several different protocols with different group lists and allowed force components. All calculations in these runs used $K_{sp} \parallel = 1.0$, $K_{sp} \perp = 0.2$, and $\mathrm{E_{tol}} = \tilde{\mathrm{F}}_{\mathrm{tol}} = 10^{-4}$.

It became clear that the asymmetry was due to artificial bounds created by the choice of the frozen/unfrozen region. We proceeded to determine the convergence of the calculation for several different parameters which are presented in the following series of tables.

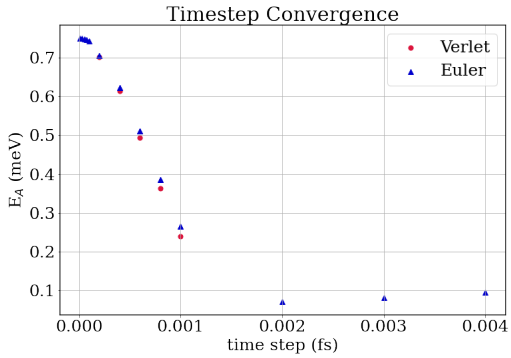

Fig. 1: Convergence plot for energy barrier as a function of timestep. The two convergence regions for the timestep was initialy troubling; however, we later determined that the small timestep region was artificial convergence due to insufficient change in position between steps.

After the rigorous series of simulations, we were confident that we had determined the convergence of the NEB calculations and found the best set of parameters for our study of hydrogen induced degradation. A small series of similar test were performed for the first few hydrogen energy barriers. These confirmed our choice of parameters.

NEB Initial and Final States

Previous studies have presented an accurate description of hydrogen in a-Si:H, where hydrogen is located in either of two classes: a deep trap, a hydrogen atom bound to an silicon atom; or a shallow trap, a hydrogen at an interstitial Si-Si bond center.[11–15] Following this model, we organized our NEB to calculations into two classes: the energy barriers for the breaking of a Si-H bond and the energy barriers for hopping between interstitial sites. The interstitial hopping barriers were calculated with initial and final states taken from the $V_H(z)$ hydrogen-energy calculations, such that the H atom moves in the z direction by approximately one Si-Si bond length, away from the interface. The bond-breaking barriers were calculated by developing an algorithm that scanned the heterojunction stacks to find all mono-hydride Si-H bonds. We identified the mono-hydride Si-H bonds by the coupled criteria that the hydrogen was separated from a single nearest Si by a bond length of about $1.50\mathring{A}$, equal to the previously reported bond length values [1, 16–18], while this Si was not bonded to a second hydrogen. It was also confirmed that the hydrogen was not at a bond center by checking for multiple Si neighbors within the cutoff distance. The mono-hydride Si-H were chosen as initial configurations for the NEB analysis. For the final configurations the hydrogen was moved from this mono-hydride bond to a neighboring bond-centered position. To remain consistent with established Si-H-Si configurations, the two Si atoms were simultaneously displaced by $0.45\mathring{A}$ along the direction of the bond. The energies of the initial and final states were then minimized using the FIRE minimizer to an energy tolerance of 10^{-3}eV before commencing the NEB analysis. A typical minimum energy path MEP for breaking a hydrogen bond is shown in Fig.2. After developing and establishing the validity of this method we proceeded to compute the energy

Table 2: **Number of NEB Atoms and Others Frozen or Unfrozen.**

Num NEB atoms	Num Replicas	FE_A(eV)	RE_A(eV)	Non NEB atoms frozen
16	16	0.368	0.240	Yes
16	16	0.111	0.111	No
1	16	0.767	0.767	Yes
1	16	0.111	0.111	No

Table 3: **Simulation Box Size and Number of Atoms**

Sim Box	Num NEB atoms	FE_A(eV)	RE_A(eV)
2x2x3	95	0.678	0.678
3x3x3	215	0.678	0.678
4x4x4	511	0.678	0.678

Table 4: **Spring Constants**

Num NEB atoms	K_{sp} $\parallel$	K_{sp} $\perp$	FE_A(eV)	RE_A(eV)
215	0.1	0.2	0.678	0.678
215	0.5	0.2	0.678	0.678
215	1.0	0.2	0.678	0.678
215	2.5	0.2	0.678	0.678
215	5.0	0.2	0.678	0.678
215	10.0	0.2	0.678	0.678
215	20.0	0.2	0.678	0.678

Table 5: **Number of Replicas**

Num NEB atoms	Number of Replicas	FE_A(eV)	RE_A(eV)
215	64	0.692	0.692
215	32	0.690	0.690
215	16	0.678	0.678
215	8	0.628	0.628
215	4	0.422	0.422

barriers for 657 initial-final state pairs for the breaking of Si-H bonds, and for more than 2000 initial-final state pairs for interstitial hopping. We determined the energy barriers for both the forward and backward direction of these processes.

Many reservoir simulations

The results of the H-potential showed no lateral variation; therefore, we concluded that a 1D model could properly capture effects of the potential energy gradient. Fig.3 shows the 1D energy landscape for a hydrogen atom at the interface. The deep well of the bonded state followed by the many shallow wells of the interstitial matrix provided the basis for a dynamical model where each energy minimum was considered a reservoir each with a flow of hydrogen in and out to the adjacent reservoirs.

The mathematical description of this model is a system of N coupled linear differential equations, see Eq.1.

$$\begin{aligned}
\tfrac{\partial}{\partial t}N_1 &= \quad k_{2,1}N_2 - k_{1,2}N_1 \\
\tfrac{\partial}{\partial t}N_2 &= k_{1,2}N_1 + k_{3,2}N_3 - (k_{2,3}+k_{2,1})N_2 \\
\tfrac{\partial}{\partial t}N_C &= k_{2,3}N_2 + k_{4,3}N_4 - (k_{3,2}+k_{3,4})N_3 \\
&\vdots \\
\tfrac{\partial}{\partial t}N_N &= \quad k_{N,N-1}N_{N-1} - k_{N-1,N}N_N
\end{aligned} \tag{1}$$

Table 6: **Timestep: Euler integrator**

Timestep (ps)	Num NEB atoms	Num Replicas	FE_A(eV)	RE_A(eV)
1.0e-05	215	17	0.750	0.750
2.5e-05	215	17	0.749	0.749
5.0e-05	215	17	0.748	0.748
7.5e-05	215	17	0.745	0.745
0.0001	215	17	0.742	0.742
0.0002	215	17	0.705	0.705
0.0004	215	17	0.623	0.623
0.0006	215	17	0.511	0.511
0.0008	215	17	0.386	0.386
0.001	215	17	0.265	0.265
0.002	215	17	0.071	0.071
0.004	215	17	0.095	0.095

Table 7: **Timestep: Verlet integrator**

Timestep (ps)	Num NEB atoms	Num Replicas	FE_A(eV)	RE_A(eV)
0.0002	215	17	0.702	0.702
0.0004	215	17	0.614	0.614
0.0006	215	17	0.494	0.494
0.0008	215	17	0.363	0.363
0.001	215	17	0.240	0.240

Table 8: **Energy Tolerance**

Timestep (ps)	Num NEB atoms	E Tol eV	FE_A(eV)	RE_A(eV)
0.0004	16	10^{-3}	0.636	0.636
0.0004	16	10^{-5}	0.636	0.636
0.0004	16	10^{-6}	0.636	0.636
0.0004	16	10^{-7}	0.113	0.113
0.0004	16	10^{-8}	0.114	0.114

The computational model for Eq.1 incorporated the H-potential as a series of forward and reverse rates corresponding to E_A that differed by $\approx$ 0.15eV. Fig.4 shows the results of these simulations. For a series of graded barriers the probability of a hydrogen returning to the interface becomes negligible. From classical Boltzmann statistics the relative probability of finding a particle in one of two states is given by

$$\frac{P(\epsilon_1)}{P(\epsilon_2)} = \frac{e^{-\beta\epsilon_1}}{e^{-\beta\epsilon_2}} = e^{-\beta(\epsilon_1-\epsilon_2)} \tag{2}$$

where $\beta = \frac{1}{k_B T}$. If we consider the mean values of E_{Drift}, $\mu = 0.41$eV, and E_{Return}, $\mu = 0.58$eV, at room temperature the relative probability of a free hydrogen drifting out deeper into the bulk is about 1000 times greater than hopping back towards the interface. When a hydrogen is n interstitial sites away from the interface the probability of returning to the interface is $\approx (1000)^n$. Fig.4 shows plots of the simulations preformed using [3-6] reservoirs. The negligible return probability for a hydrogen after escaping the interface reduces the number of influential barriers from 2x(atomic layers) to 3.

A similar process was used to validate the approximation of the reverse energy gradient by the three barrier model. We simulated the hydrogen dynamics for up to 9 atomic layers, using a stochastic solution to the coupled differential equations. We again found that the presence of a gradient over numerous barriers could be well approximated using a single "effective" third barrier. The algorithm used for the many reservoir simulations was derived from *Numerical Recipes:*

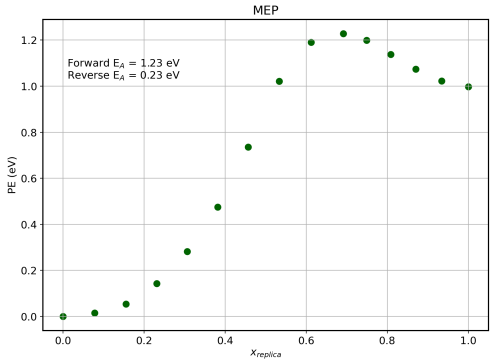

Fig. 2: Minimum energy path for the process of breaking an Si-H bond.

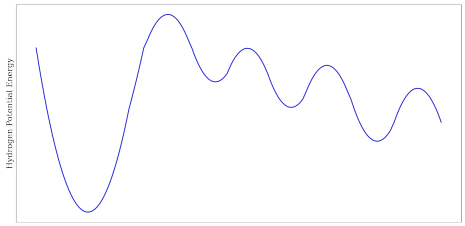

Fig. 3: Animation of the potential energy surface for a hydrogen atom at the interface. The slope of the shallow sites signifies the H-potential driving the hydrogen from the interface toward the bulk.

The Art of Scientific Computing 17.7 Stochastic Simulation of Chemical Reaction Networks.

Rates

Rates were determined using the Arrhenius equation.

$$k = Ae^{-\frac{E_A}{k_B T}} \tag{3}$$

Using T=300 K gives $k_B T \approx 0.026eV$. FTIR data shows that the Si-H stretching mode absorbs a photon with $\tilde{\nu} = \frac{1}{\lambda} \approx 2000\frac{1}{cm}$ which gives $A = \nu \approx 6 \times 10^{13}$Hz. To focus on the relevant time scales, A was scaled to $\frac{1}{\text{weeks}}$ resulting in $A = 1.6 \times 10^1 8(weeks)^{-1}$. This gave the following expression for the rates used.

$$k(E_A) = (1.65 \times 10^1 8)e^{-\frac{E_A}{0.026(eV)}}(weeks)^{-1} \tag{4}$$

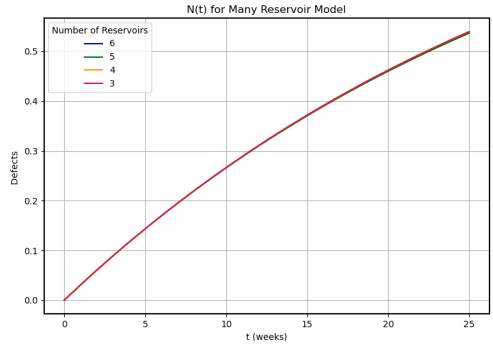

Fig. 4: Defect growth over time from stochastic solutions to Eq.1, for 3, 4, 5, and 6 reservoirs. Due to the potential energy gradient the probability of a hydrogen returning to the interface becomes negligible after only a few interstitial sites.

IPR and Partial Charge

Localization of a Kohn-Sham wavefunction can be determined by inverse participation ratio (IPR) quantity that is calculated using the following expression:

$$IPR_n = \frac{\Sigma_{i=1}^{I} a_{ni}^4}{(\Sigma_{i=1}^{I} a_{ni}^2)^2} \tag{5}$$

where a_{ni} is the coefficient of i^{th} basis set in the n^{th} Kohn-Sham wavefunction obtained from DFT calculations. In order to find the maximum contribution of each atom inside a supercell in localization of Kohn-Sham wavefunctions, we defined a quantity named IPR_k as follows:

$$IPR_k = MAX_{n,j}^{k}\{IPR_{nkj}\} \tag{6}$$

where IPR_{nkj} is obtained from the rearrangement of equation 5

$$IPR(\Psi_n) = \frac{\Sigma_{k=1}^{K}\Sigma_{j=1}^{J} a_{nkj}^4}{(\Sigma_{k=1}^{K}\Sigma_{j=1}^{J} a_{nkj}^2)^2} \tag{7}$$

Fig.5(a) shows the IPR_{nkj}s, calculated for all Kohn-Sham orbitals obtained by DFT as a function of their energy for a typical c-Si/a-Si:H stack.

Partial charges within DFT framework were obtained using the Lowdin population analysis where the plain wave basis-set wavefunctions were projected to the atomic orbitals of atoms inside the supercell.

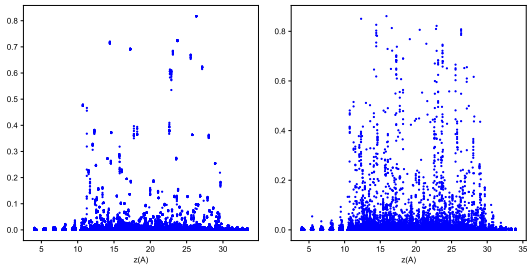

Fig. 5: IPR on atoms at the c-Si/a-Si:H interface and in aSi:H regions before and after an H atom is taken out of a dangling bond and placed at a Si-Si bond center.

References

[1] Unruh, D., Meidanshahi, R.V., Goodnick, S.M., Csányi, G., Zimányi, G.T.: Gaussian approximation potential for amorphous Si:H. Phys. Rev. Materials **6**, 065603 (2022). https://doi.org/10.1103/PhysRevMaterials.6.065603

[2] Giannozzi, P., *et al.*: Quantum espresso: a modular and open-source software project for quantum simulations of materials. J. Phys.: Condens. Matter **21**, 395502 (2009)

[3] Giannozzi, P., *et al.*: Advanced capabilities for materials modelling with quantum espresso. J. Phys.: Condens. Matter **29**, 465901 (2017)

[4] Giannozzi, P., *et al.*: Quantum espresso toward the exascale. J. Chem. Phys. **152**, 154105 (2020)

[5] Perdew, J.P., Burke, K., Ernzerhof, M.: Generalized gradient approximation made simple. Phys. Rev. Lett. **77**, 3865–3868 (1996)

[6] Marzari, N., Vanderbilt, D., De Vita, A., Payne, M.C.: Thermal contraction and disordering of the al(110) surface. Phys. Rev. Lett. **82**, 3296–3299 (1999). https://doi.org/10.1103/PhysRevLett.82.3296

[7] Methfessel, M., Paxton, A.T.: High-precision sampling for brillouin-zone integration in metals. Phys. Rev. B **40**, 3616–3621 (1989). https://doi.org/10.1103/PhysRevB.40.3616

[8] Van Vechten, J.A.: Activation enthalpy of recombination-enhanced vacancy migration in si. Phys. Rev. B **38**, 9913–9919 (1988). https://doi.org/10.1103/PhysRevB.38.9913

[9] Van Vechten, J.A.: Enthalpy of vacancy migration in si and ge. Phys. Rev. B **10**, 1482–1506 (1974). https://doi.org/10.1103/PhysRevB.10.1482

[10] Bartók, A.P., Kermode, J., Bernstein, N., Csányi, G.: Machine learning a general-purpose interatomic potential for silicon. Phys. Rev. X **8**, 041048 (2018). https://doi.org/10.1103/PhysRevX.8.041048

[11] Herring, C., Johnson, N.M., Van de Walle, C.G.: Energy levels of isolated interstitial hydrogen in silicon. Phys. Rev. B **64**, 125209 (2001). https://doi.org/10.1103/PhysRevB.64.125209

[12] De Wolf, S., Olibet, S., Ballif, C.: Stretched-exponential a-si:hc-si interface recombination decay. Applied Physics Letters **93**(3), 032101 (2008) https://doi.org/10.1063/1.2956668. https://doi.org/10.1063/1.2956668

[13] Santos, P.V., Johnson, N.M., Street, R.A., Hack, M., Thompson, R., Tsai, C.C.: Hydrogen migration and electronic carriers in a-si:h. Phys. Rev. B **47**, 10244–10260 (1993). https://doi.org/10.1103/PhysRevB.47.10244

[14] Kakalios, J., Street, R.A., Jackson, W.B.: Stretched-exponential relaxation arising from dispersive diffusion of hydrogen in amorphous silicon. Phys. Rev. Lett. **59**, 1037–1040 (1987). https://doi.org/10.1103/PhysRevLett.59.1037

[15] Shlesinger, M.F., Montroll, E.W.: On the williams & watts function of dielectric relaxation. Proceedings of the National Academy of Sciences **81**(4), 1280–1283 (1984). https://doi.org/10.1073/pnas.81.4.1280

[16] Herring, C., Johnson, N.M., Van de Walle, C.G.: Energy levels of isolated interstitial hydrogen in silicon. Phys. Rev. B **64**, 125209 (2001). https://doi.org/10.1103/PhysRevB.64.125209

[17] Panzarini, G., Colombo, L.: Hydrogen diffusion in silicon from tight-binding molecular dynamics. Phys. Rev. Lett. **73**, 1636–1639 (1994). https://doi.org/10.1103/PhysRevLett.73.1636

[18] Tersoff, J.: Modeling solid-state chemistry: Interatomic potentials for multicomponent systems. Phys. Rev. B **39**, 5566–5568 (1989). https://doi.org/10.1103/PhysRevB.39.5566